Acta Biomaterialia 71 (2018) 388–397

Contents lists available at ScienceDirect

Acta Biomaterialia

journal homepage: www.elsevier.com/locate/actabiomat

Full length article

Characterizing viscoelastic mechanical properties of highly compliant polymers and biological tissues using impact indentation

Aleksandar S. Mijailovic [a,1], Bo Qing [b,1], Daniel Fortunato [c], Krystyn J. Van Vliet [b,d,*]

[a] Department of Mechanical Engineering, Massachusetts Institute of Technology, Cambridge, MA 02139, USA
[b] Department of Biological Engineering, Massachusetts Institute of Technology, Cambridge, MA 02139, USA
[c] John A. Paulson School of Engineering and Applied Sciences, Harvard University, Cambridge, MA 02138, USA
[d] Department of Materials Science and Engineering, Massachusetts Institute of Technology, Cambridge, MA 02139, USA

ARTICLE INFO

Article history:
Received 30 September 2017
Received in revised form 19 January 2018
Accepted 15 February 2018
Available online 1 March 2018

Keywords:
Viscoelasticity
Mechanical characterization
Indentation
Biomechanics
Polymer mechanics

ABSTRACT

Precise and accurate measurement of viscoelastic mechanical properties becomes increasingly challenging as sample stiffness decreases to elastic moduli <1 kPa, largely due to difficulties detecting initial contact with the compliant sample surface. This limitation is particularly relevant to characterization of biological soft tissues and compliant gels. Here, we employ impact indentation which, in contrast to shear rheology and conventional indentation, does not require contact detection *a priori*, and present a novel method to extract viscoelastic moduli and relaxation time constants directly from the impact response. We first validate our approach by using both impact indentation and shear rheology to characterize polydimethylsiloxane (PDMS) elastomers of stiffness ranging from 100 s of Pa to nearly 10 kPa. Assuming a linear viscoelastic constitutive model for the material, we find that the moduli and relaxation times obtained from fitting the impact response agree well with those obtained from fitting the rheological response. Next, we demonstrate our validated method on hydrated, biological soft tissues obtained from porcine brain, murine liver, and murine heart, and report the equilibrium shear moduli, instantaneous shear moduli, and relaxation time constants for each tissue. Together, our findings provide a new and straightforward approach capable of probing local mechanical properties of highly compliant viscoelastic materials with millimeter scale spatial resolution, mitigating complications involving contact detection or sample geometric constraints.

Statement of significance

Characterization and optimization of mechanical properties can be essential for the proper function of biomaterials in diverse applications. However, precise and accurate measurement of viscoelastic mechanical properties becomes increasingly difficult with increased compliance (particularly for elastic moduli <1 kPa), largely due to challenges detecting initial contact with the compliant sample surface and measuring response at short timescale or high frequency. By contrast, impact indentation has highly accurate contact detection and can be used to measure short timescale (glassy) response. Here, we demonstrate an experimental and analytical method that confers significant advantages over existing approaches to extract spatially resolved viscoelastic moduli and characteristic time constants of biological tissues (*e.g.*, brain and heart) and engineered biomaterials.

1. Introduction

The performance of biomaterials used in diverse engineering applications can be either limited or enabled by mechanical properties of the material. For example, in the tissue engineering field, replacements for bone and cartilage require specific load-bearing capabilities to function properly and remain biomechanically stable [1–5]. There is also significant interest in developing

* Corresponding author at: Departments of Materials Science and Engineering and Biological Engineering, Massachusetts Institute of Technology, 77 Massachusetts Ave, Cambridge, MA 02139, USA.
E-mail address: krystyn@mit.edu (K.J. Van Vliet).
[1] These authors contributed equally.

https://doi.org/10.1016/j.actbio.2018.02.017
1742-7061/

synthetic materials that recapitulate the mechanical behavior of so called "soft tissues" such as brain tissue, which are more mechanically compliant and more susceptible to injury, for applications unrelated to tissue engineering or regenerative medicine. Instead, these brain tissue simulants can be used to evaluate new protective helmets during ballistic testing, optimize robotic surgery techniques, and guide the design of brain implant devices to minimize the risk of injury [6–8]. Accurate measurement of the mechanical properties of compliant materials is relevant not only for replacing or mimicking tissues, but also for elucidating the role of material mechanics in disease diagnosis or progression. Several cell types have demonstrated sensitivity to both biochemical and mechanical cues [9–14], and some diseases involving brain tissue, including glioma, multiple sclerosis or autism spectrum disorder, exhibit structural changes within the tissue that may alter local mechanical properties [15–19]. Whether any such mechanical differences can be detected and may modulate biological and behavioral functions (*e.g.,* neuronal connectivity and cognition) remain open and important questions.

The above applications of brain tissue-scale mechanical properties motivate the need for methods that precisely and accurately characterize such parameters. Unfortunately, several experimental challenges arise when the material of interest is of such low stiffness, particularly when the material is expected to deform in a rate-dependent or viscoelastic manner. Uniaxial and biaxial tensile experiments are prone to sample damage and experimental artifacts associated with the requirements for sample clamping and uniform cross-sectional geometry [20,21]. Thus, conventional approaches for characterizing mechanical properties of highly compliant, viscoelastic materials have been relegated chiefly to dynamic frequency sweep tests or creep and stress relaxation tests, commonly using macroscale shear rheology, compressive tests, or indentation-based methods [22,23]. However, one significant limitation of these existing approaches is the requirement of contact detection between the measurement probe and sample surface, prior to the application of the prescribed load or displacement. Accurate contact detection becomes extremely challenging for materials of very low stiffness (<10 kPa), due in part to limited signal-to-noise sensitivity of commercial force transducers and to the inertia and finite compliance of the instrument load frame [24–27]. These limitations result frequently in inadvertent "prestress" or premature compression of the sample prior to the initiation of the controlled experiment, and can introduce significant experimental variation depending on sample thickness and degree of nonlinear elastic response [19,26,28]. Furthermore, at short deformation timescales associated with the polymer "glassy" or "instantaneous" response, idealized step-loads and step-displacements can contribute errors in measurements in creep or relaxation experiments. Similarly, shear rheology is constrained by a maximum measurable frequency due to machine limitations (*e.g.*, frame inertia upon reversal of shearing displacement), making the glassy response challenging to measure. While time-temperature superposition may be used to widen the accessible frequency or timescale and thus approach the glassy response [29], this method is limited in measuring high frequency response (*i.e.*, low temperatures) of hydrated biological tissues as they will freeze at low temperatures. Additional limitations of macroscale shear rheology include stringent constraints for the sample geometry, need for an attachment method such as sandpaper or glue to prevent slip [30], and lack of spatial resolution, which can be important when investigating heterogeneous, hierarchically structured materials like biological tissues. On the other hand, indentation-based methods provide spatial resolution of inferred mechanical properties, but can also include other practical challenges such as probe-sample adhesion and inaccurate contact detection [31].

We have demonstrated previously that impact indentation can be used to quantify the response of biological soft tissues, as well as polymers engineered as potential tissue simulants, to concentrated impact loading [6–8]. This approach is distinct in operation from indentation load-depth hysteresis or creep and relaxation experiments, and does not rely on detecting contact *a priori*. Previous studies of brain, liver, heart, and gels reported this impact response empirically, quantifying the penetration resistance, energy dissipation capacity, and energy dissipation rate, but could not relate the deformation response to more conventional and widely reported mechanical properties of the material such as viscoelastic moduli. Here, we present a novel analytic method for characterizing viscoelastic moduli and relaxation time constants from impact indentation experiments, and highlight the key limitations of conventional approaches that are addressed by our technique. We first validate our novel approach by utilizing both impact indentation and macroscale shear rheology to measure the properties of polydimethylsiloxane (PDMS) elastomers and demonstrate strong agreement between the two methods. We then apply impact indentation to characterize the equilibrium shear moduli, instantaneous shear moduli, and relaxation time constants of brain, liver, and heart tissue. Importantly, this approach enables spatially resolved measurement of viscoelastic moduli for polymers or tissues of nominal stiffness or equilibrium shear moduli <1 kPa.

2. Theory

Indentation generally includes the controlled deformation of a planar sample surface by a three-dimensional object or probe of known geometry and mechanical properties, such that the probe displacement can be attributed unambiguously to sample deformation and then related directly to mechanical properties of that material through knowledge or measurement of the force and assumptions of specific constitutive laws of the sample material. The specific subset of this deformation of present interest, impact of rigid spheres on a linearly viscoelastic semi-infinite half-space, has been studied previously [32–34]. Our present derivation extends this analysis to the impact of a viscoelastic body by a pendulum with a flat cylindrical punch indenter (Fig. 1(A)). This reflects the impact indenter design, which confers deformation of the sample material through displacement of a pendulum-mounted probe at known pendulum velocities. A torque balance on the pendulum (see Supplementary Information, S1) may be rewritten as a force balance between the sum of external forces $F_{ext}(t)$ and the pendulum inertia, pendulum damping, gravity, and the force from Hertzian contact of a flat punch indenter on a linearly viscoelastic half-space [35]:

$$F_{ext}(t) = m_{eff}\frac{d^2u}{dt^2} + b\frac{du}{dt} + k_g u + \frac{4R}{(1-\upsilon)}\int_0^t G(t-t')\frac{du(t')}{dt'}dt' \qquad (1)$$

where u is the linear displacement of the indenter, m_{eff} is an effective mass related to the moment of inertia of the pendulum, b is intrinsic pendulum damping coefficient, k_g is an equivalent gravitational "stiffness," R is the radius of the indenter, υ is the Poisson's ratio of the sample, and $G(t)$ is the shear relaxation function of the sample. The constants R, m_{eff}, b, and k_g are properties of the instrumented indenter, and can be determined experimentally (see Supplementary Information, S3). Elastomers and biological soft tissues are often idealized as incompressible materials, meaning that υ approaches 0.5 and, more importantly, is constant in time. Therefore, if the loading conditions are known, measuring the indenter's displacement enables quantification of the material constitutive law in the form of $G(t)$, as illustrated in Fig. 1(B).

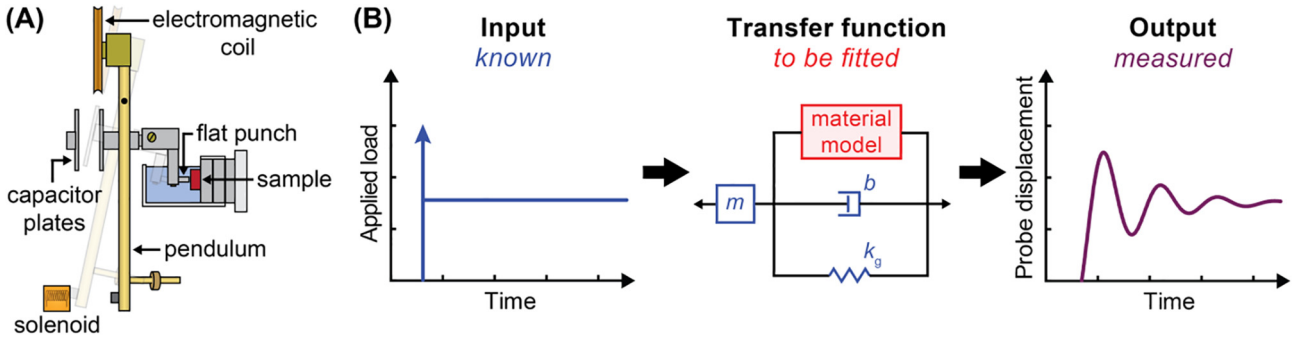

Fig. 1. (A) Schematic of pendulum-based instrumented indenter (Micro Materials Ltd.) for conducting impact indentation experiments. The faded, transparent image represents the initial starting position of the pendulum, while the solid image represents the position of the pendulum immediately prior to impacting the sample. (B) Framework for quantifying viscoelastic material properties via impact indentation. The known input and measured output are related by a transfer function defined by the pendulum mass m, damping coefficient b, gravitational stiffness k_g, and a viscoelastic constitutive model that describes the material response. Because m, b, and k_g are calibrated beforehand, the parameters associated with a given material model can be fitted to the displacement response of the sample.

The external load is approximated as the sum of the inertial impulse from impact [34] and a constant load applied throughout the experiment, as reflects the expected loading history of the instrument used in these impact indentation experiments. With impact at $t = 0$,

$$F_{ext}(t) = m_{eff} v_{in} \delta(t) + F_{el} H(t) \tag{2}$$

where v_{in} is the impact velocity, $\delta(t)$ is the Dirac delta function, F_{el} is the load applied by the electromagnetic coil, and $H(t)$ is the Heaviside step function. The impact event provides an objectively identifiable contact point even in compliant samples, and a sufficiently high prescribed force F_{el} results in maintained contact between the indenting probe and sample surface after the initial impact event or impulse.

In contrast to the direct output obtained from creep, stress relaxation, or rheology experiments, the constitutive behavior $G(t)$ of a material is not obtained from a fit to the raw data such as displacement vs. time. Instead, the form of $G(t)$ is assumed, and the measured displacement response as a function of time is fitted to the solution of Eq. (1) to obtain the parameters associated with $G(t)$. For instance, in the examples below we assumed the linear viscoelastic Standard Linear Solid (SLS) constitutive model, which is described by the relaxation function as:

$$G(t) = G_\infty + (G_0 - G_\infty) e^{-t/\tau} \tag{3}$$

where G_∞ is the equilibrium shear modulus, G_0 is the instantaneous shear modulus, and τ is the characteristic relaxation time constant. Additionally, G_∞ and G_0 may be estimated using limiting conditions. At long timescales, the impacted material's relaxation modulus balances the applied load and gravity force acting on the pendulum, and Eq. (1) becomes

$$F|_{t=\infty} = u|_{t=\infty} \left(\frac{4R}{(1-\nu)} G_\infty + k_g \right) \tag{4}$$

Therefore, G_∞ may be estimated by using the final depth of the probe, applied load, and known constants of the material and calibrated instrument. At shorter timescales, the system has an underdamped response similar to that of a spring-mass-damper system, with a natural frequency related to the instantaneous stiffness, effective mass, and damping factor of the system. We estimated G_0 using Eq. (5), which relates G_0 to the natural frequency of the oscillations ω_d. The frequency depends on the instantaneous stiffness of the material, gravity on the pendulum, equivalent mass of the pendulum, and the damping factor ζ:

$$\omega_d \approx \sqrt{\frac{\frac{4R}{(1-\nu)} G_0 + k_g}{m_{eff}} (1 - \zeta^2)} \tag{5}$$

3. Materials and methods

3.1. Impact indentation

The modified configuration of the instrumented indenter (NanoTest, Micro Materials Ltd.) used to conduct impact indentation experiments on compliant materials is depicted in Fig. 1(A). Full details of the experimental procedure and calibration of the instrument parameters m_{eff}, b, and k_g have been described in previous work [7,8,24,36], and the instrumentation design (hardware, operation, and signal acquisition) in the current study is the same as that used in Qing et al. and Canovic et al. [8,24]. Briefly, a pendulum supporting a cylindrical flat punch probe impacts the sample at a known velocity and oscillates until the impact energy is fully dissipated. The instrumented indenter records the displacement of the probe throughout the impact process. Fig. 2(A)–(D) illustrates an example of the probe displacement output, along with the corresponding velocity, acceleration, and jerk profiles that can be calculated by taking the first, second, and third derivative of displacement with respect to time, respectively. Jerk, the time derivative of acceleration or da/dt, will show discontinuities during steps in acceleration or sudden changes in the slope of the acceleration, such as during impact. We defined zero displacement as the position at which the probe made contact with the sample surface at an impact velocity v_{in}. To identify this contact point x_0, we first examined the jerk profile (Fig. 2(D)) to identify a sudden change in direction and sharp decrease, as indicated by the red circle. As expected, this point coincided with a noticeable change in slope of the acceleration profile (Fig. 2(C)), reflecting that contact in many samples is approximately concurrent with an instance of zero acceleration and maximum velocity. Note that we did not directly assume x_0 to be the point of maximum velocity because of the potential for inherent dissipation by the pendulum. Additionally, the jerk profile appeared smoother when the stiffness of the sample was <1 kPa, and thus the contact point was more difficult to identify accurately and objectively as polymer or tissue stiffness decreased below this magnitude, for the given instrument design and internal dissipation (see Supplementary Information, S4).

We employed a stainless steel cylindrical flat punch probe with a radius of 1 mm to characterize all materials, with applied impact loads ranging from 3.5 to 15 mN and corresponding to impact velocities between 3 and 8 mm/s. We could not access the highest loads and velocities for the most compliant samples considered herein, owing simply to the limited maximum measurable indentation depth of the instrument. During mechanical characterization, PDMS samples were immersed fully in 150 mM NaCl

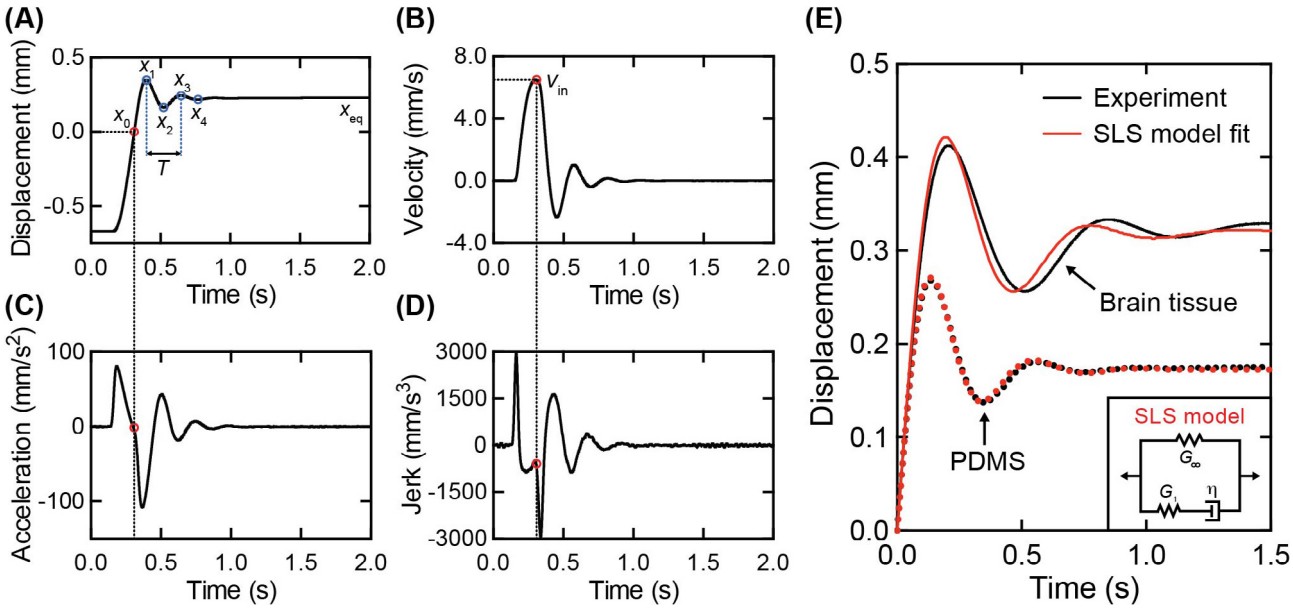

Fig. 2. (A) Probe displacement is recorded as a function of time during the impact process, and the corresponding (B) velocity, (C) acceleration, and (D) jerk profile can be calculated. The acceleration and jerk profiles are used to determine when contact between the probe and sample occurs, as indicated by the red circles. The blue circles in (A), which correspond to the amplitudes of the underdamped oscillation, are used to determine the damping ratio and period T of the system. (E) Representative experimental data (black) and SLS model fits (red) of the displacement vs. time response for porcine brain tissue (solid curve) and PDMS (dotted curve). Inset: Schematic of the SLS constitutive model for linear viscoelasticity. (For interpretation of the references to colour in this figure legend, the reader is referred to the web version of this article.)

phosphate buffered saline (PBS) containing 3% Pluronic® F108 to minimize adhesion to the probe, while biological soft tissues were immersed in nutrient media (Hibernate®-A) to maintain tissue hydration and structural integrity. We have demonstrated previously that fluid drag forces negligibly contributed to the overall damping of the system, verifying that testing in these specific fluids did not affect the measured mechanical response [6,7].

3.2. Impact analysis to extract mechanical properties

We obtained the material constants G_∞, G_0, and τ by fitting the solution to Eq. (1) to the measured displacement as a function of time, examples of which are shown in Fig. 2(E). While the form of the solution to Eq. (1) may be written explicitly, the constants must be calculated by residue theory, and thus there is no closed form solution in terms of the viscoelastic moduli, relaxation time constant, system parameters, loading conditions and initial conditions. For simplicity, we solved Eq. (1) by performing a numerical inverse Laplace transform of its transfer function:

$$\bar{U}(s) = \frac{\bar{F}(s)}{\bar{P}(s)} = \frac{v_{in} + \frac{F_{el}}{m_{eff}s}}{s^2 + \frac{b}{m_{eff}}s + \frac{4R}{m_{eff}(1-\upsilon)}\left(G_\infty + \frac{(G_0 - G_\infty)s}{\left(s+\frac{1}{\tau}\right)}\right) + \frac{k_g}{m_{eff}}} \quad (6)$$

where s is complex frequency, and $U(s)$, $F(s)$, and $P(s)$ are the Laplace transformed displacement, external load and characteristic polynomial, respectively. The parameters v_{in}, F_{el} , m_{eff}, b, and k_g were known, and the polymers or tissues were assumed to be incompressible (Poisson's ratio $\upsilon = 0.5$), as is commonly assumed for polymers such as PDMS and soft tissues [22,37–39]. We then extracted G_∞, G_0, and τ using a nonlinear curve fit (MATLAB) of the experimental time-displacement data (Fig. 2(E)). We estimated goodness of fit between the model-predicted and measured displacement vs. time response through calculation of R^2. Although this is an inexact metric of fit quality for nonlinear models [40], it provides a useful first approximation that can be compared across datasets. To ensure our data were not overfitted, we quantified the covariance between variables G_∞, G_0, and τ, and graphically examined relationships between the variables (Supplementary Information, S9).

Additionally and separately, we estimated G_∞ and G_0 using limiting conditions for analysis of the same data. Specifically, we used Eq. (4) to estimate G_∞ based on the final depth of the probe and known applied load, and estimated G_0 using Eq. (5) by measuring the natural frequency of the impact response and the damping factor ζ. We calculated the damping factor by logarithmic decrement using the period T and local maxima and minima of the displacement profile (x_1, x_2, x_3, and x_4 in Fig. 2(A)).

3.3. Macroscale shear rheology

We conducted oscillatory shear rheology experiments at 25 °C using a parallel plate rheometer (Anton Paar MCR 501) with a plate diameter of 10 mm to characterize the macroscale viscoelastic mechanical properties of PDMS. We confirmed that frequency sweeps from 0.1 to 100 rad/s at 1% shear strain were in the linear viscoelastic regime using strain sweep experiments. We calculated shear storage moduli G' and loss moduli G'' as a function of frequency via the rheometer vendor software. We then converted rheological data to a Prony series through curve fitting using a constrained nonlinear least squares optimization scheme in MATLAB (see Supplementary Information, S6).

3.4. Polymer synthesis

We synthesized and used PDMS-based elastomers in validation experiments. CY52-276 PDMS (Dow Corning®) is a two-component silicone kit, and allowed for easy tunability of elastomer crosslink density and stiffness. Part A contained the prepolymer base, and Part B contained the catalyst. We prepared mixtures of three distinct mass-to-mass ratios of Part A to Part B (1.25:1, 1:1, and 1:1.2) and hereafter refer to these three compositions as polymers A, B, and C, respectively. After degassing under vacuum to remove

air bubbles and pouring into silanized petri dishes, we cured the CY52-276 samples at 80 °C overnight. We then cut samples of cured PDMS, immersed in PBS containing 3% Pluronic® F108, with a surgical punch. Since the mixtures produced highly compliant and adhesive samples, the Pluronic® F108 helped enable clean detachment of the silicone from the Petri dish [41]. The volume of mixture that was prepared controlled the final thickness of the sample. We prepared samples of 2 mm and 6 mm thickness for mechanical testing via macroscale oscillatory shear rheology and impact indentation, respectively. These polymers are stable in typical lab air environments. However, we mechanically characterized them in aqueous fluid herein both to minimize probe adhesion (through modification of the fluid composition) and to confirm the minimal impact of viscous drag on the measured response of other samples that are most appropriately characterized in fully hydrated states (*e.g.*, soft tissues obtained from mammalian organs).

3.5. Tissue procurement

We harvested whole porcine brains from healthy adult pigs at a local stockyard in Massachusetts. Liver and heart organs were harvested from healthy adult Sprague-Dawley rats obtained from the Division of Comparative Medicine at MIT. All experiments involving tissues followed the University IACUC protocol and the NIH guidelines for animal care. Tissue preparation for mechanical characterization via impact indentation has been detailed in previous work [7,8]. We sliced brain tissue into 6 mm thick sections exhibiting flat and parallel surfaces, and immediately stored samples in Hibernate®-A, a CO_2-independent nutrient medium for adult neural tissue. For both liver and heart, we prepared tissue discs of 8 mm diameter and thickness of 3–5 mm using a surgical punch, and stored these discs in Krebs-Henseleit buffer. We conduced mechanical characterization experiments between 3 and 48 h *post mortem*, with samples immersed fully in the corresponding aqueous media. Over this duration, the measured impact response did not vary detectably.

3.6. Statistical analysis of tissue properties

To determine whether impact indentation distinguished viscoelastic constants G_∞, G_0, and τ between different tissues, we conducted a series of Mann-Whitney tests for each parameter between each tissue (significance at $p < 0.05$). The Mann-Whitney rank-based test was chosen due to the small number of measurements ($n = 4$, 8, 12 for liver, heart and brain, respectively).

4. Results

4.1. Validation of impact indentation technique on PDMS

We characterized three PDMS elastomers of varying crosslink density and anticipated stiffness (PDMS A, B, and C, as denoted in order of increasing crosslink density). We fit the impact responses of each PDMS elastomer, assuming an SLS model, to extract G_∞, G_0, and τ. The fits matched well to the experimental data, with R^2 values exceeding 0.95 (see Supplementary Information, S5). While we acknowledge that R^2 is an inadequate goodness of fit for nonlinear models [40], it provides a useful first estimate of model agreement across experimental datasets, such as experiments with different loads and materials. The dotted curves in Fig. 2(E) illustrate an SLS model fit for PDMS B, which exhibited an intermediate stiffness. Although we examined each sample under multiple loading conditions (see Supplementary Information, S7), Fig. 3 illustrates results acquired at the lowest applied impact velocity. We found G_∞ to span an order of magnitude among these three polymers, whereas G_0 spanned a factor of four and τ was similar among all samples. Specifically, PDMS A exhibited mean G_∞ of 400 Pa, G_0 of 5.5 kPa, and τ of 0.050 s; PDMS B exhibited mean G_∞ of 2.2 kPa, G_0 of 10.4 kPa, and τ of 0.055 s; and PDMS C exhibited mean G_∞ of 4.8 kPa, G_0 of 19.9 kPa, and τ of 0.052 s. As expected, the measured moduli correlated directly with the crosslink density of the PDMS elastomer.

Fig. 3 also compares G_∞, G_0, and τ obtained from impact indentation, shown in blue, to those obtained from macroscale shear rheology, shown in gray. The viscoelastic moduli at both very long timescales and very short timescales agreed strongly between the two characterization techniques for all three PDMS samples, as illustrated by Fig. 3(A) and (B), respectively. Additionally, the characteristic time constants agreed reasonably well between the two methods (Fig. 3(C)), though a robust comparison with rheology is difficult because a glassy plateau at high frequencies was not observed in those experiments and multiple time constants were necessary to fit the shear rheology experimental data. The time constant associated with the largest weight in the Prony series was used for comparison against the time constant measured by impact indentation.

4.2. Characterization of biological soft tissues

An important application of such a validated approach is the mechanical characterization of biological soft tissues. Brain, liver, and heart tissues are relatively compliant as compared to mineralized tissues such as bone, and thus more difficult to mechanically characterize accurately. We characterized mammalian tissues from all three organs via impact indentation to obtain viscoelastic properties. The response predicted by the fitting to Eq. (1) matched reasonably well to the experimental impact data for these biological samples, with R^2 exceeding 0.9 for all cases. An example demonstrating the quality of fit for brain tissue is shown by the solid curves in Fig. 2(E) (more extensively in Supplementary Information, S5), and Table 1 shows the magnitudes of G_∞, G_0, and τ as determined by an SLS model fit (Eqs. (1) and (6); see Methods). We also confirmed lack of covariance in our measured G_∞, G_0, and τ, suggesting that the variables were likely not overfitted or coupled strongly (Supplementary Information, S9). While the standard deviation of the mean was appreciable among replicate experiments for a given property and tissue source, we attributed this variation chiefly to natural variation among tissue samples ($n = 2$ to 4 samples per species per tested condition), and also to variation in tissue structure and corresponding mechanical response at distinct locations in the same sample ($N = 2$ to 4 replicate impact indentation experiments at well-spaced positions in a given sample). Statistical power was sufficiently high to confirm statistically significant differences between liver and heart and between brain and heart for G_∞, G_0, and τ (Mann-Whitney U, $p < 0.05$). Liver and brain exhibited significantly different time constants (Mann-Whitney U, $p < 0.05$), but did not exhibit significantly different G_∞ or G_0 (Mann-Whitney U, $p > 0.05$).

Murine heart tissue exhibited the greatest stiffness at short deformation timescales as expressed by the instantaneous shear modulus, with G_0 of ~ 11 kPa exceeding that of porcine brain (2.4 kPa) and murine liver (2.1 kPa) tissues (Table 1). Heart tissue also exhibited higher stiffness at longer timescales described by the equilibrium shear modulus, with G_∞ of $\sim$3 kPa exceeding that of brain (0.1 kPa) and liver (0.2 kPa) tissues by approximately an order of magnitude. Note that because the tissues were sourced from animal species, we do not claim here any inferences from the relative magnitudes attributed to organ tissue type; those differences could be attributed reasonably to a variety of factors including species-dependent or animal age-dependent tissue

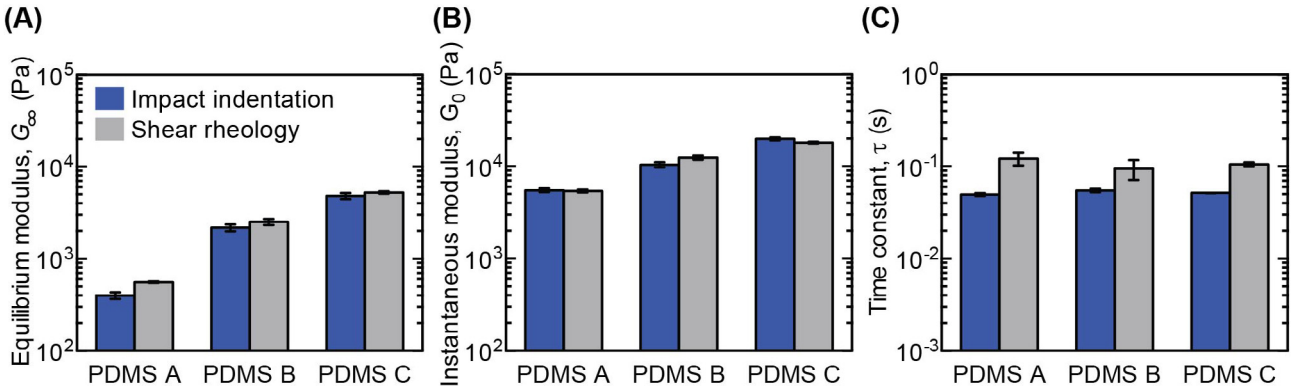

Fig. 3. Comparison of the (A) equilibrium shear modulus, (B) instantaneous shear modulus, and (C) relaxation time constant calculated by fitting impact indentation data (blue) with an SLS model and fitting oscillatory shear rheology data (gray). Three PDMS elastomers of varying crosslink density were examined. Results are represented as mean ± standard deviation (n = 3 replicate measurements for each experimental technique). (For interpretation of the references to colour in this figure legend, the reader is referred to the web version of this article.)

Table 1
Viscoelastic mechanical properties of biological soft tissues measured via impact indentation, calculated via Eq. (1). Data represented as mean ± standard deviation (n = 12, 4, and 8 replicate measurements for brain, liver, and heart tissue, respectively).

Soft tissue	Equilibrium shear modulus, G_∞ (Pa)	Instantaneous shear modulus, G_0 (Pa)	Time constant, τ (ms)
Brain (Porcine)	125 ± 25	2410 ± 550	115 ± 8
Liver (Murine)	190 ± 97	2075 ± 393	220 ± 17
Heart (Murine)	2885 ± 1505	11035 ± 3266	103 ± 8

structure and properties, and systematic comparisons among tissues would consider a single species source. Additionally, we note that the characteristic viscoelastic time constants indicated that liver tissue relaxed noticeably more slowly than the other soft tissues, exhibiting a time constant τ of ~200 ms as compared to ~100 ms for the other two tissues. These comparisons simply illustrate the capacity to obtain three distinct viscoelastic descriptors of soft tissues, with sufficiently high precision and statistical power that one can draw comparisons among hydrated tissue types or testing conditions.

Analytical estimates for G_∞ and G_0 based on Eqs. (3) and (4), respectively, also agreed reasonably well with the results for those two properties obtained from the SLS model fits. The G_∞ estimates were 60 ± 29 Pa, 145 ± 97 Pa, and 2.6 ± 1.3 kPa, and the G_0 estimates were 1.9 ± 0.6 kPa, 2.0 ± 0.4 kPa, and 11.4 ± 3.0 kPa for brain, liver and heart, respectively. This serves as a secondary validation of the approach, through independent analysis of the same data with associated analytical approximations that use only a portion of the displacement vs. time response (see Theory).

5. Discussion

5.1. Advantages of impact indentation over conventional techniques

Impact indentation provides several advantages over conventional techniques, for which accurate and precise measurements of macroscale viscoelastic mechanical properties become increasingly difficult with increasing compliance. One of the most significant challenges for macroscale shear rheology and quasistatic indentation of highly compliant samples is the accurate and objective identification of the contact commencement between the probe and the sample. Inaccuracy in contact point identification can lead to overestimates in measured moduli if the polymer or tissue is strain stiffening over that range of actual material deformation [42]. However, impact indentation allows for a clearly observable change in the acceleration and jerk of the probe (Fig. 2(C) and (D)), providing more accurate contact detection. Shear rheology also requires that a nonzero compressive load be applied to the material prior to data acquisition, to provide sufficient friction between the plate and sample; that requirement can lead to a non-uniform pre-stressed state that may alter the measured shear moduli [19,26]. Pre-stresses are obviated in impact indentation, as the deformation commences upon impact.

The impact response also improves analysis of short timescale glassy behavior as the natural frequency of the oscillation is directly related to the viscoelastic properties of the material. This frequency may be calculated exactly from the (imaginary component of the) poles of the system's transfer function (Eq. (6)), and may be estimated by Eq. (5). By contrast, measurement of short timescale, so-called glassy behavior of the material may be more difficult in conventional creep compliance and stress relaxation experiments. Such experiments may not be able to achieve sufficiently "instantaneous" steps of applied displacement or load, and instrument timescale resolution is limited to how quickly these "steps" may be applied.

An additional advantage of the present approach, which can be advantageous for materials such as soft tissues that can also exhibit appreciable "stickiness" or adhesion, is the flat punch probe geometry. Adhesion introduces error in instrumented indentation and AFM-enabled indentation (including probe-based creep and stress relaxation experiments) when a spherical indenter is used; the contact area with the sphere varies naturally with indentation depth, and unpredictably so when the extent of probe-material adhesion is not well established [31,43]. In contrast, impact indentation with a flat punch geometry maintains constant contact area between the probe surface and sample surface, minimizing adhesive energy dissipation, provided that slip does not occur at the material surface. Furthermore, because the probe does not retract beyond the original surface plane of the undeformed material during the entire impact process, contact and traction at the probe-material interface are maintained under the impact indentation

conditions reported herein. Thus, artifacts such as tensile loading on the sample when retracting from an adhesive surface and reducing the effective contact are not contributors to the measured response. While the small but finite rotation of the probe may lead to sliding at the surface or misalignment of the probe and surface during impact, these effects are likely negligible as vertical displacements in the present pendulum-based impact experiments are approximately three orders of magnitude smaller than horizontal displacements into the material. As in conventional indentation-based techniques, impact indentation also allows for local measurement of viscoelastic properties on the length scale of the probe dimensions. This spatial resolution can provide a significant advantage over macroscale shear rheology, dynamic mechanical analysis, and tension tests that only give average properties of the bulk sample, particularly for structurally heterogeneous samples such as biological tissues. In this study, we measured properties on the millimeter length scale; in principle, lower length scales may be measured by using a smaller probe. However, a practical limit to this spatial resolution is anticipated as the probe radius decreases, artifacts due to stress concentrations at the edges of the flat punch will increase in relative contribution to the measured response.

While we have demonstrated this approach specifically for a flat punch probe geometry and an SLS material constitutive model, impact indentation may be generalized readily to other probe geometries and material models. Any linear material model may be used with the solving and fitting methods described herein by replacing the form of the relaxation function $G(t)$. Non-linear material models may also be used, but in that case Eq. (1) becomes non-linear and may not be solved with Laplace transforms. Spherical probe geometry may also be implemented (see Supplementary Information, S2), again resulting in a non-linear equation. This invalidates the Laplace transform technique such that the governing differential equation must be solved in the time domain. The spherical probe geometry confers the advantage of avoiding stress concentration at edges, but may be subject to significant adhesive effects due to change in contact area over the course of the data acquisition period.

5.2. Validation of impact indentation against shear rheology on compliant PDMS

We validated the viscoelastic parameters of engineered, compliant polymers obtained by impact indentation through comparison with oscillatory shear rheology. In all PDMS samples tested, the contact point was identifiable clearly from the acceleration and jerk (Fig. 2), and curve fits matched the experimental data well when fitted to only three variables (see Supplementary Information, S5). We did not observe an impulse in the acceleration or a discontinuity in the velocity as would be expected from a rigid body impact, for example. Rather, we observed a clear shift in the acceleration and a discontinuity in the jerk (Fig. 2(C) and (D)), demonstrating the instantaneous response of the impacted material during probe-material contact. For the material surface, the impact corresponds to an instantaneous change in the material surface velocity, assuming that the inertial effects in the material are negligible. Thus, the delta function or impulsive "load" in Equation (3) may be interpreted physically as an initial condition at $t = 0^+$ in the pendulum-material system, as the material response does not exist prior to impact. The improved contact detection is likely due to instantaneous glassy response of the sample during impact, which is effectively stiffer and therefore more easily measurable than the response in a typical low velocity contact detection procedure.

Comparison of the measured PDMS viscoelastic properties indeed validated impact indentation against shear rheology. The equilibrium shear modulus measured by indentation was in agreement with the fit obtained from macroscale shear rheology experiments (Fig. 3(A)). Interestingly, we observed that the computed G_∞ was slightly lower when obtained from macroscale shear rheology compared to that obtained from impact indentation, with the largest difference for the most compliant sample, PDMS A. This comparison is consistent with our hypothesis that impact indentation would quantify a lower G_∞ than rheology because accurate contact detection afforded by the former approach avoids compressive pre-stress artifacts known to affect rheology and conventional indentation methods [26,42]. While the instantaneous shear modulus also agreed well between those methods (Fig. 3(B)), it is more difficult to definitively compare the magnitudes of G_0 because there existed no observable plateau in the high frequency rheology data that would be assigned unambiguously to G_0. Moreover, comparing time constants between techniques is not meaningful because the entire frequency range is not measured in rheology, and because multiple time constants must be used to obtain a good fit (see Supplementary Information, S6).

5.3. Measurement of tissue viscoelastic properties by impact indentation and challenges at very low stiffness

We also demonstrated that impact indentation may be used to measure the viscoelastic mechanical properties of fully immersed and hydrated biological soft tissues, including those obtained from mammalian brain, liver, and heart (Table 1). Further, we demonstrated that the analytical estimates for G_∞ and G_0 (from Eqs. (4) and (5) agreed well with the values obtained from fitting an SLS model, indicating that physical reasoning governing short and long timescale material response agrees with analytical solutions. These estimates are useful in model fitting, as they may be used as initial guesses for G_∞ and G_0 during iterative fitting of the transfer function. Note that in our study, we did not use these estimates of initial guesses as this could have invalidated comparisons between the model and Eqs. (4) and (5). The analytical estimate of G_0 may also be used to determine whether use of multiple time constants overfits the data, as the glassy modulus should remain insensitive to the number of time constants represented in the transient response. The relation in Eq. (5) is also remarkable as it allows measurement of G_0 independent of applied load, analogous to measurement of elastic modulus by wave propagation speed.

It is notable that contact was clearly detectable for impact indentation in heart tissue, exhibiting instantaneous changes in slope in acceleration and discontinuities in the jerk profiles that was similar to the engineered polymers. The contact point was less visually obvious for measurements on brain and liver tissue, but still detectable (see Supplementary Information, S4). In all tissues, the identifiable contact point likely improved measurement of G_∞. The equilibrium shear modulus is most commonly and straightforwardly measured by other techniques, and therefore it is an appropriate property to assess accuracy of our approach. We found that G_∞ calculated from the impact indentation response was in reasonable agreement with the admittedly wide range of literature reports for all tissues measured herein. For the liver and brain tissue, the expected range of G_∞ according to prior reports is on the order of several hundred Pa [19,22,26,28,44]. For brain tissue specifically, Gefen et al. conducted indentation creep on *ex vivo* porcine brain with a spherical indenter, reporting G_∞ of approximately 450 Pa; this was the same order of magnitude as we determined for this mechanical property, but nearly fourfold higher [45]. Additionally, we had conducted shear rheology previously (Fig. S6) on the same porcine brain tissue source as those used in our present impact indentation experiments [24] (see Supplementary Information, S10). From those shear rheology data, we fitted a Prony series to obtain G_∞ of 208 ± 20 Pa, which was

close to but higher than our impact indentation measurement of 125 ± 25 Pa. Furthermore, we demonstrated that increasing axial compressive strain increased both G_∞ and G_0 of porcine brain tissue measured by shear rheology (Fig. S7), confirming results from previous studies attributed to the pre-strain or pre-stress effect [19,26]. This suggests that accurate contact detection via impact indentation resulted in lower magnitude of measured G_∞ by avoiding compressive pre-stress of the tissue [19,26,42]. Heart tissue is more structurally anisotropic than these tissues at the length scales considered in this study [46], and we did not design this study to probe mechanical anisotropies in this tissue. As the complex and three-dimensional stress field of indentation does not facilitate direct measurement of anisotropic moduli, we consider the viscoelastic properties reported herein for heart tissue to be order of magnitude estimates that would be refined further through consideration of potential anisotropies.

Along with accurate contact detection, experimental time scales must be sufficiently long to accurately measure G_∞. The porcine brain measurements by Gefen et al. [45] as well as our own rheology experiments were conducted at considerably longer timescales (10 s of seconds), yet still measured a stiffer response as compared to impact indentation. These results suggest that our long-timescale stiffness measurements (i.e., G_∞) were not substantially overestimated due to our shorter experimental procedure, at least compared to other experimental artifacts. Nevertheless, we note that measurements over extended timescales are certainly possible for impact indentation, and may be pursued in future work if necessary for the materials or properties of interest.

In addition to agreement in G_∞, we found that G_0 for porcine brain tissue also agreed well with the range expected in the literature. Chatelin et al. [22] provided a review of available data for brain tissue acquired by various approaches, from which we observed that the magnitude of G' measured by rheology at high frequencies (~100 Hz) was in the range of 500–1000 Pa and not yet plateaued. Our results thus corresponded to prior studies within an order of magnitude. Furthermore, the time constant we obtained for brain tissue agreed with that reported by Prange et al. [47], in which stress relaxation experiments fitted with two time constants exhibited a dominant time constant at 100 ms (and a secondary time constant of approximately 3 s). Those researchers reported what was termed a maximum modulus of ~500 Pa, which was significantly less than our measured magnitude of $G_0 \sim 2100$ Pa. However, the time resolution available to Prange et al. was only on the order of 0.01 s, which may not be small enough to measure the true G_0; in contrast, our approach determined G_0 from the natural frequency of the damped oscillation. In previous work by Gefen et al., the authors found a short timescale modulus G_1 of 1200 Pa by fitting a two-branch Prony series to their creep measurements conducted with a spherical indenter [45]. They noted that this G_1 value approaches G_0, but did not reach it due to the inability to achieve a perfect step in load during the experiment, an artifact common to creep and stress relaxation tests. Fitting our rheological measurements on porcine brain [24], we found that $G_0 = 780 \pm 66$ Pa, with measurements up to ~15 Hz (Supplementary Information, S10). The magnitude of G_0 obtained from rheology was lower than in impact indentation, likely because short-timescale behavior was not captured by such rheological measurements.

In summary, impact indentation provides advantages in measuring viscoelastic moduli at both long and short timescales. In impact indentation, measurements are less heavily influenced by the shortest measureable timescales of the instrument and the timescale over which "steps" in load or displacement, or maximum frequency, may be achieved for creep or stress relaxation tests, respectively, and thus are not expected to underestimate G_0. At all timescales, accurate contact detection eliminates the artifact of pre-stress or pre-strain, and thus should not overestimate G_∞ (as well as G_0) for the linear deformation regime.

While we observed good agreement in G_∞ for brain, liver, and heart tissues, we note that measured moduli increased with increasing impact velocity and load; equivalently, those measured moduli increased with higher maximum penetration depths and strains (see Supplementary Information, S7). We attribute these trends to nonlinear, strain-stiffening material behavior that would occur at sufficiently high deformation strains and particularly at stress concentrations at the edge of the indenter–material interface. Thus, the linear range should be established by "sweeping" the applied load to identify the onset of this asymptotic behavior, similar to an amplitude strain sweep in macroscale shear rheology [24,39]. In this study, all data presented were measured at the lowest measurable load, and thus were either within or approached the linear approximation (see Supplementary Information, S7).

In addition to material nonlinearity, the intrinsic pendulum parameters m_{eff}, b, and k_g may increase measurement error for highly compliant materials if the signal contribution by these parameters to the displacement-time response significantly exceeds the contribution from the material response. These parameters could be optimized for improved instrument design and displacement profile design in future studies. For example, in our measurements for porcine brain tissue, the material "stiffness" term $\frac{4R}{(1-\nu)}G_\infty$ was several times smaller than the pendulum parameter k_g, so by Eq. (4), a small error in contact point leads to significant error in measured relaxation modulus (i.e., k_g amplifies the small contact point error). While we maintained the capacity to measure the equilibrium moduli of brain tissue due to accurate contact detection, this issue can also be mitigated by altering the instrument design (*e.g.*, decreasing the pendulum k_g) or by simply by increasing the radius of the probe. Similarly, the intrinsic pendulum damping b can be reduced to minimize contributions to the measured dissipative response.

While the pendulum parameters may affect the measurement of G_∞ significantly depending on the relative viscoelastic properties of the sample, Eq. (5) indicates that measurement of G_0 should be relatively insensitive to pendulum design for tissues. This robustness is due to the typically small damping factors (<0.3) and to the common observation that $G_0 \gg G_\infty$ for soft tissues. Under these conditions, the pendulum parameter k_g does not contribute strongly to the measured signal. We also note that we neglected analysis of inertial effects in the impacted materials because the timescale of deformation was much longer than the time required for stress waves to propagate the thickness of the material [48]. It remains possible that some energy was dissipated through wave propagation, and we have not addressed the extent of this possible error.

5.4. Future work

We have demonstrated that impact indentation can be used to accurately measure the viscoelastic properties of engineered polymers and biological tissues, even when the samples are of low mechanical stiffness that confers complications in conventional rheological experiments. Through straightforward fitting of the displacement-time response, this approach obviates the need for *a priori* detection of contact with the sample and accesses well understood viscoelastic parameters of appropriate viscoelastic constitutive laws. While this study demonstrates that impact indentation may be used to measure linear viscoelastic mechanical properties of compliant materials including biological tissues, future work is necessary to optimize fully the instrument design,

methodology, and modeling of the material behavior. Improved assessment of this approach as compared with other conventional techniques, and across a wider range of polymers, tissues, and testing conditions, will also facilitate robust measurements of accuracy. In the present work, we did not optimize design of the instrument, a pendulum-based indenter, including parameters such as the moment of inertia, damping properties, and gravitational "stiffness" (or m_{eff}, b, and k_g, respectively). Such design optimization would likely improve the accuracy in measuring highly compliant materials, chiefly by increasing the material response signal compared to the intrinsic damping and gravitation effects of the pendulum, as well as by improving the accuracy of contact detection.

The timescales of our impact indentation experiments were on the order of several seconds, and therefore, we did not consider long-term relaxation. However, straightforward changes to the experimental procedure could improve characterization of long-term viscoelastic behavior. This technique has the capability of extending timescales to 100 s to 1000 s of seconds, increasing the frequency window if it is relevant to an application of interest. Therefore, impact indentation has the capacity to measure the same information as a conventional creep experiments at long timescales, but with significantly improved resolution to detect glassy behavior. Further studies should establish the most effective experimental procedure to precisely and accurately calculate viscoelastic moduli and relaxation behavior at all timescales.

Our analysis thus far has been limited to the SLS constitutive model of viscoelastic deformation, other isotropic, linear viscoelastic constitutive models may be implemented straightforwardly. Other material behavior such as linear poroelastic deformation has been investigated by indentation [49,50]; extending the present analysis to include such behavior should be feasible in principle, provided that a load-displacement response may be calculated iteratively to fit the experimental data. Under sufficiently large deformation exceeding that reported herein (Supplementary information, S7), the assumption of material linearity may not hold for polymers and soft tissues, and nonlinear constitutive behavior should be taken into account [47,51,52]. In general, however, the complex stress and strain fields imposed by indentation present challenges in accurate measurement of nonlinear elastic as well as structurally and mechanically anisotropic materials [53].

6. Conclusions

In this study, we provided an analytical model for impact indentation, facilitating measurement of viscoelastic moduli and relaxation time constants of highly compliant polymers and biological soft tissues with shear relaxation moduli as low as 100 s of Pa. This approach confers advantages of millimeter scale resolution, minimal sample preparation, improved contact detection, and minimal artifacts due to probe-sample adhesion. While similar to creep compliance and stress relaxation experiments at long timescales, impact indentation provides the additional capacity to measure the glassy response, and therefore characterizes a more complete viscoelastic response over extended timescales compared to those methods. We also note that impact indentation is generalizable to different material constitutive models and different probe geometries, but that an assumed material model is necessary to measure the shear relaxation moduli of the material. These findings motivate future work to apply and extend this approach to a wider range of polymers and tissues, including for comparisons within tissues and among tissue sources of key viscoelastic properties that are correlative with tissue structure and disease state.

Acknowledgements

This research was supported by the U.S. Army through the Institute for Soldier Nanotechnologies under Contract W911NF-07-D-0004. B.Q. acknowledges the National Defense Science and Engineering Graduate Fellowship, and K.J.V.V. gratefully acknowledges the Michael and Sonya Koerner Professorship.

Appendix A. Supplementary data

Supplementary data associated with this article can be found, in the online version, at https://doi.org/10.1016/j.actbio.2018.02.017.

References

[1] R.E. Neuendorf, E. Saiz, A.P. Tomsia, R.O. Ritchie, Adhesion between biodegradable polymers and hydroxyapatite: relevance to synthetic bone-like materials and tissue engineering scaffolds, Acta Biomater. 4 (2008) 1288–1296, https://doi.org/10.1016/j.actbio.2008.04.006.
[2] C. Correia, S. Bhumiratana, L.-P. Yan, A.L. Oliveira, J.M. Gimble, D. Rockwood, D. L. Kaplan, R.A. Sousa, R.L. Reis, G. Vunjak-Novakovic, Development of silk-based scaffolds for tissue engineering of bone from human adipose-derived stem cells, Acta Biomater. 8 (2012) 2483–2492, https://doi.org/10.1016/j.actbio.2012.03.019.
[3] S. Yang, K.-F. Leong, Z. Du, C.-K. Chua, The design of scaffolds for use in tissue engineering. Part I. Traditional factors, Tissue Eng. 7 (2001) 679–689, https://doi.org/10.1089/107632701753337645.
[4] S.J. Bryant, K.S. Anseth, Controlling the spatial distribution of ECM components in degradable PEG hydrogels for tissue engineering cartilage, J. Biomed. Mater. Res. A. 64 (2003) 70–79, https://doi.org/10.1002/jbm.a.10319.
[5] W. Zhao, X. Jin, Y. Cong, Y. Liu, J. Fu, Degradable natural polymer hydrogels for articular cartilage tissue engineering, J. Chem. Technol. Biotechnol. 88 (2013) 327–339, https://doi.org/10.1002/jctb.3970.
[6] Z.I. Kalcioglu, M. Qu, K.E. Strawhecker, T. Shazly, E. Edelman, M.R. VanLandingham, J.F. Smith, K.J. Van Vliet, Dynamic impact indentation of hydrated biological tissues and tissue surrogate gels, Philos. Mag. 91 (2011) 1339–1355, https://doi.org/10.1080/14786435.2010.512574.
[7] Z.I. Kalcioglu, R.a. Mrozek, R. Mahmoodian, M.R. VanLandingham, J.L. Lenhart, K.J. Van Vliet, Tunable mechanical behavior of synthetic organogels as biofidelic tissue simulants, J. Biomech. 46 (2013) 1583–1591, https://doi.org/10.1016/j.jbiomech.2013.03.011.
[8] B. Qing, K.J. Van Vliet, Hierarchical design of synthetic gel composites optimized to mimic the impact energy dissipation response of brain tissue, Mol. Syst. Des. Eng. 1 (2016) 290–300, https://doi.org/10.1039/C6ME00051G.
[9] D.E. Discher, P. Janmey, Y.-L. Wang, Tissue cells feel and respond to the stiffness of their substrate, Science. 310 (2005) 1139–1143, https://doi.org/10.1126/science.1116995.
[10] R.G. Wells, The role of matrix stiffness in regulating cell behavior, Hepatology. 47 (2008) 1394–1400, https://doi.org/10.1002/hep.22193.
[11] N.D. Leipzig, M.S. Shoichet, The effect of substrate stiffness on adult neural stem cell behavior, Biomaterials. 30 (2009) 6867–6878, https://doi.org/10.1016/j.biomaterials.2009.09.002.
[12] Y. Sun, C.S. Chen, J. Fu, Forcing stem cells to behave: a biophysical perspective of the cellular microenvironment, Annu. Rev. Biophys. 41 (2012) 519–542, https://doi.org/10.1146/annurev-biophys-042910-155306.
[13] A.S. Zeiger, B. Hinton, K.J. Van Vliet, Why the dish makes a difference: quantitative comparison of polystyrene culture surfaces, Acta Biomater. 9 (2013) 7354–7361, https://doi.org/10.1016/j.actbio.2013.02.035.
[14] A. Jagielska, A.L. Norman, G. Whyte, K.J. Van Vliet, J. Guck, R.J.M. Franklin, Mechanical environment modulates biological properties of oligodendrocyte progenitor cells, Stem Cells Dev. 21 (2012) 2905–2914, https://doi.org/10.1089/scd.2012.0189.
[15] C.F. Lucchinetti, W. Brück, J.E. Parisi, B. Scheithauer, M. Rodriguez, H. Lassmann, W. Bruck, J.E. Parisi, B. Scheithauter, M. Rodriguez, H. Lassmann, Heterogenity of multiple sclerosis lesions: implication for the pathogenesis of demyelination, Ann Neurol. 47 (2001) 707–717, https://doi.org/10.1002/1531-8249(200006).
[16] A. Kutzelnigg, C.F. Lucchinetti, C. Stadelmann, W. Brück, H. Rauschka, M. Bergmann, M. Schmidbauer, J.E. Parisi, H. Lassmann, Cortical demyelination and diffuse white matter injury in multiple sclerosis, Brain. 128 (2005) 2705–2712, https://doi.org/10.1093/brain/awh641.
[17] P. Curatolo, R. Bombardieri, S. Jozwiak, Tuberous sclerosis, Lancet. 372 (2008) 657–668, https://doi.org/10.1016/S0140-6736(08)61279-9.
[18] L. Meikle, D.M. Talos, H. Onda, K. Pollizzi, A. Rotenberg, M. Sahin, F.E. Jensen, D. J. Kwiatkowski, A mouse model of tuberous sclerosis: neuronal loss of Tsc1 causes dysplastic and ectopic neurons, reduced myelination, seizure activity, and limited survival, J. Neurosci. 27 (2007) 5546–5558, https://doi.org/10.1523/JNEUROSCI.5540-06.2007.
[19] K. Pogoda, L. Chin, P.C. Georges, F.J. Byfield, R. Bucki, R. Kim, M. Weaver, R.G. Wells, C. Marcinkiewicz, P.a. Janmey, Compression stiffening of brain and its

effect on mechanosensing by glioma cells, New J. Phys. 16 (2014) 75002, https://doi.org/10.1088/1367-2630/16/7/075002.
[20] K. Miller, K. Chinzei, Mechanical properties of brain tissue in tension, J. Biomech. 35 (2002) 483–490, https://doi.org/10.1016/S0021-9290(01)00234-2.
[21] X. Nie, B. Song, Y. Ge, W.W. Chen, T. Weerasooriya, Dynamic tensile testing of soft materials, Exp. Mech. 49 (2009) 451–458, https://doi.org/10.1007/s11340-008-9133-5.
[22] S. Chatelin, A. Constantinesco, R. Willinger, Fifty years of brain tissue mechanical testing: from in vitro to in vivo investigations, Biorheology. 47 (2010) 255–276, https://doi.org/10.3233/BIR-2010-0576.
[23] B. Rashid, M. Destrade, M.D. Gilchrist, Mechanical characterization of brain tissue in tension at dynamic strain rates, J. Mech. Behav. Biomed. Mater. 33 (2014) 43–54, https://doi.org/10.1016/j.jmbbm.2012.07.015.
[24] E.P. Canovic, B. Qing, A.S. Mijailovic, A. Jagielska, M.J. Whitfield, E. Kelly, D. Turner, M. Sahin, K.J. Van Vliet, Characterizing multiscale mechanical properties of brain tissue using atomic force microscopy, impact indentation, and rheometry, J. Vis. Exp. 115 (2016) 1–12, https://doi.org/10.3791/54201.
[25] M. Hrapko, J.a.W. Van Dommelen, G.W.M. Peters, J.S.H.M. Wismans, Characterisation of the mechanical behaviour of brain tissue in compression and shear, Biorheology. 45 (2008) 663–676, https://doi.org/10.3233/BIR-2008-0512.
[26] M. Ayyildiz, S. Cinoglu, C. Basdogan, Effect of normal compression on the shear modulus of soft tissue in rheological measurements, J. Mech. Behav. Biomed. Mater. 49 (2015) 235–243, https://doi.org/10.1016/j.jmbbm.2015.05.011.
[27] K. Tan, S. Cheng, L. Jugé, L.E. Bilston, Characterising soft tissues under large amplitude oscillatory shear and combined loading, J. Biomech. 46 (2017) 1060–1066, https://doi.org/10.1016/j.jbiomech.2013.01.028.
[28] G. Mattei, A. Tirella, G. Gallone, A. Ahluwalia, Viscoelastic characterisation of pig liver in unconfined compression, J. Biomech. 47 (2014) 2641–2646, https://doi.org/10.1016/j.jbiomech.2014.05.017.
[29] F. Shen, T.E. Tay, J.Z. Li, S. Nigen, P.V.S. Lee, H.K. Chan, Modified Bilston nonlinear viscoelastic model for finite element head injury studies, J. Biomech. Eng. 128 (2006) 797–801, https://doi.org/10.1115/1.2264393.
[30] S. Nicolle, J. Palierne, D. Lyon, On the efficiency of attachment methods of biological soft tissues in shear experiments, J. Mech. Behav. Biomed. Mater. 14 (2012) 158–162, https://doi.org/10.1016/j.jmbbm.2012.05.002.
[31] D.M. Ebenstein, Nano-JKR force curve method overcomes challenges of surface detection and adhesion for nanoindentation of a compliant polymer in air and water, J. Mater. Res. 26 (2011) 1026–1035, https://doi.org/10.1557/jmr.2011.42.
[32] S.C. Hunter, The Hertz problem for a rigid spherical indenter and a viscoelastic half-space, J. Mech. Phys. Solids. 8 (1960) 219–234, https://doi.org/10.1016/0022-5096(60)90028-4.
[33] H.H. Calvit, Numerical solution of the problem of impact of a rigid sphere onto a linear viscoelastic half-space and comparison with experiment, Int. J. Solids Struct. 3 (1967) 951–966, https://doi.org/10.1016/0020-7683(67)90021-2.
[34] C.P. Chen, R.S. Lakes, Design of viscoelastic impact absorbers: optimal material properties, Int. J. Solids Struct. 26 (1990) 1313–1328, https://doi.org/10.1016/0020-7683(90)90081-6.
[35] L. Cheng, X. Xia, W. Yu, L.E. Scriven, W.W. Gerberich, Flat-punch indentation of viscoelastic material, J. Polym. Sci. Part B Polym. Phys. 38 (2000) 10–22, https://doi.org/10.1002/(SICI)1099-0488(20000101)38:1<10::AID-POLB2>3.0.CO;2-6.
[36] G. Constantinides, C.a. Tweedie, N. Savva, J.F. Smith, K.J. Vliet, Quantitative impact testing of energy dissipation at surfaces, Exp. Mech. 49 (2009) 511–522, https://doi.org/10.1007/s11340-008-9198-1.
[37] M. Chun, M. Hoon, F. Chiong, C. Teck, Viscoelastic effects of silicone gels at the micro- and nanoscale, Procedia IUTAM. 12 (2015) 20–30, https://doi.org/10.1016/j.piutam.2014.12.004.
[38] A. Samadi-dooki, G.Z. Voyiadjis, R.W. Stout, A combined experimental, modeling, and computational approach to interpret the viscoelastic response of the white matter brain tissue during indentation, J. Mech. Behav. Biomed. Mater. 77 (2018) 24–33, https://doi.org/10.1016/j.jmbbm.2017.08.037.
[39] P.A. Janmey, P.C. Georges, S. Hvidt, Basic rheology for biologists, Methods Cell Biol. 83 (2007) 3–27, https://doi.org/10.1016/S0091-679X(07)83001-9.
[40] A. Spiess, N. Neumeyer, An evaluation of R^2 as an inadequate measure for nonlinear models in pharmacological and biochemical research : a Monte Carlo approach, BMC Pharmacol. (2010) 1–11, https://doi.org/10.1186/1471-2210-10-6.
[41] C.G.P.H. Schroen, M.A.C. Stuart, K.V.D.V. Maarschalk, A. Van Der Padt, K. Van Riet, Influence of preadsorbed block copolymers on protein adsorption: surface properties, layer thickness, and surface coverage, Langmuir 11 (1995) 3068–3074, https://doi.org/10.1021/la00008a036.
[42] J.D. Kaufman, C.M. Klapperich, Surface detection errors cause overestimation of the modulus in nanoindentation on soft materials, J. Mech. Behav. Biomed. Mater. 2 (2009) 312–317, https://doi.org/10.1016/j.jmbbm.2008.08.004.
[43] C. Hui, T. Liu, T. Salez, E. Raphael, A. Jagota, Indentation of a rigid sphere into an elastic substrate with surface tension and adhesion, Proc. R. Soc. A Math. Phys, Eng. Sci. 471 (2015), https://doi.org/10.1098/rspa.2014.0727.
[44] K. Franze, P.a. Janmey, J. Guck, Mechanics in neuronal development and repair, Annu. Rev. Biomed. Eng. 15 (2013) 227–251, https://doi.org/10.1146/annurev-bioeng-071811-150045.
[45] A. Gefen, S.S. Margulies, Are in vivo and in situ brain tissues mechanically similar?, J Biomech. 37 (2004) 1339–1352, https://doi.org/10.1016/j.jbiomech.2003.12.032.
[46] J. Li, X.Y. Luo, Z.B. Kuang, A nonlinear anisotropic model for porcine aortic heart valves, J. Biomech. 34 (2001) 1279–1289, https://doi.org/10.1016/S0021-9290(01)00092-6.
[47] M.T. Prange, S.S. Margulies, Regional, directional, and age-dependent properties of the brain undergoing large deformation, J. Biomech. Eng. 124 (2002) 244–252, https://doi.org/10.1115/1.1449907.
[48] K.L. Johnson, Contact Mechanics, Cambridge Univeristy Press, Cambridge, UK, 1985.
[49] L. Han, E.H. Frank, J.J. Greene, H.Y. Lee, H.H.K. Hung, A.J. Grodzinsky, C. Ortiz, Time-dependent nanomechanics of cartilage, Biophys. J. 100 (2011) 1846–1854, https://doi.org/10.1016/j.bpj.2011.02.031.
[50] Z.I. Kalcioglu, R. Mahmoodian, Y. Hu, Z. Suo, K.J. Van Vliet, From macro- to microscale poroelastic characterization of polymeric hydrogels via indentation, Soft Matter. 8 (2012) 3393–3398, https://doi.org/10.1039/c2sm06825g.
[51] R.A. Schapery, Nonlinear viscoelastic and viscoplastic constitutive equations based on thermodynamics, Mech. of Time-Dependent Mater. 1 (1997) 209–240, https://doi.org/10.1023/A:1009767812821.
[52] T.P. Prevost, A. Balakrishnan, S. Suresh, S. Socrate, Biomechanics of brain tissue, Acta Biomater. 7 (2011) 83–95, https://doi.org/10.1016/j.actbio.2010.06.035.
[53] M.L. Oyen, Nanoindentation of biological and biomimetic materials, Exp. Tech. 37 (2013) 73–87, https://doi.org/10.1111/j.1747-1567.2011.00716.x.